Parametric instability of a monochromatic Alfven wave: Perpendicular decay in low beta plasma

Xinliang Gao, Quanming Lu, Xing Li, Lican Shan, and Shui Wang

Citation: Phys. Plasmas **20**, 072902 (2013); doi: 10.1063/1.4816703
View online: http://dx.doi.org/10.1063/1.4816703
View Table of Contents: http://pop.aip.org/resource/1/PHPAEN/v20/i7
Published by the AIP Publishing LLC.

Parametric instability of a monochromatic Alfven wave: Perpendicular decay in low beta plasma

Xinliang Gao,[1] Quanming Lu,[1,a)] Xing Li,[2] Lican Shan,[1] and Shui Wang[1]
[1]*CAS Key Laboratory of Geospace Environment, Department of Geophysics and Planetary Science, University of Science and Technology of China, Hefei 230026, China*
[2]*Institute of Mathematics and Physics, Aberystwyth University, Aberystwyth SY23 3BZ, United Kingdom*

(Received 17 May 2013; accepted 26 June 2013; published online 29 July 2013)

Two-dimensional hybrid simulations are performed to investigate the parametric decay of a monochromatic Alfven wave in low beta plasma. Both the linearly and left-hand polarized pump Alfven waves are considered in the paper. For the linearly polarized pump Alfven wave, either a parallel or obliquely propagating wave can lead to the decay along the perpendicular direction. Initially, the parametric decay takes place along the propagating direction of the pump wave, and then the decay occurs in the perpendicular direction. With the increase of the amplitude and the propagating angle of the pump wave (the angle between the propagating direction of the pump wave and the ambient magnetic field), the spectral range of the excited waves becomes broad in the perpendicular direction. But the effects of the plasma beta on the spectral range of the excited waves in perpendicular direction are negligible. However, for the left-hand polarized pump Alfven wave, when the pump wave propagates along the ambient magnetic field, the parametric decay occurs nearly along the ambient magnetic field, and there is no obvious decay in the perpendicular direction. Significant decay in the perpendicular direction can only be found when the pump wave propagates obliquely. © *2013 AIP Publishing LLC*. [http://dx.doi.org/10.1063/1.4816703]

I. INTRODUCTION

The observations by Helios and Ulysses have revealed that large amplitude Alfven waves exist pervasively in the fast solar wind.[1–3] In the fast solar wind, both the sunward and the antisunward propagating Alfven waves are observed, and their amplitude ratio increases with the distance from the Sun,[4] which indicates the local production of sunward propagating Alfven waves. In the relatively homogeneous fast solar wind, without the large-scale velocity shears, the parametric decay is believed to play an important role in producing locally the sunward propagating waves.[4–8] The parametric decay of parallel propagating Alfven waves with a finite amplitude along the background magnetic field has been investigated in low beta plasma by both theoretical and simulation works.[6,9–14] The parametric decay of a pump Alfven wave can produce a forward ion acoustic wave and a backward Alfven wave. The growth rate of the parametric decay is found to increase with the increase of the amplitude of the pump wave and the decrease of the plasma beta.[15] Kinetic effect is also considered to play an important role in the parametric decay. The ions can be heated by the resulted ion acoustic wave; at the same time, the growth rate of the instability and the range of the unstable modes are changed due to ion dynamics.[16–21] In particle-in-cell (PIC) simulations of the parametric decay, which treat kinetically both ions and electrons, the modified two-stream instability is also found to be unstable, and the electrons are then heated.[14]

Although the parametric decay of a monochromatic Alfven wave has been thoroughly investigated by one-dimensional (1-D) simulations, few studies have been devoted to studying the instability with two-dimensional (2-D) simulations. 2-D analytical theory[22] and simulations based on magnetohydrodynamics (MHD)[23–25] have shown that the parametric decay of parallel propagating pump Alfven waves is essentially a one-dimensional process, and after the saturation, a turbulent cascade transverse to the field occurs due to the anti-propagating Alfven waves. With a 2-D hybrid simulation model, Matteini *et al.*[26] studied the decay instability of a linearly polarized Alfven wave propagating obliquely to the ambient magnetic field in low beta plasma, and they found that the instability results in broad band oblique spectra of coupled Alfvenic and compressive modes with large perpendicular wavevectors. In this paper, with 2-D hybrid simulations, we investigate the parametric decay for both a linearly and left-hand polarized pump Alfven waves in low beta plasma, and their different behaviors in the perpendicular decay are compared.

This paper is organized as follows. In Sec. II, the plasma parameters and simulation model are described. The simulation results are illustrated in Sec. III. A summary and discussions are given at last.

II. SIMULATION MODEL

A 2-D hybrid simulation model with periodic boundary condition is used to study the parametric decay of a monochromatic Alfven wave in low beta plasma. In hybrid simulations, the ions are treated kinetically, while the electrons are described as massless fluid.[27–29] The simulations are performed in the $x - y$ plane, and the units of space and time are

a)Author to whom correspondence should be addressed. Electronic mail: qmlu@ustc.edu.cn

TABLE I. The simulation parameters for Run 1–9.

Run	β_i	$\delta B_z/B_0$	$\theta_{k_0B_0}(^\circ)$	Polarization
1	0.01	0.1	0	Linear
2	0.01	0.2	0	Linear
3	0.01	0.3	0	Linear
4	0.04	0.3	0	Linear
5	0.09	0.3	0	Linear
6	0.01	0.2	15	Linear
7	0.01	0.2	30	Linear
8	0.01	0.2	0	Left-hand
9	0.01	0.2	30	Left-hand

c/ω_{pp} (where c/ω_{pp} is the proton inertial length) and Ω_p^{-1} (where $\Omega_p = eB_0/m_pc$ is the proton gyro-frequency, and B_0 is the ambient magnetic field), respectively. We initialize the system using a monochromatic linearly polarized Alfven wave $\mathbf{\delta B_w} = \delta B\cos(\omega t - k_0x)\mathbf{e_z}$ (where ω and k_0 are the frequency and wave number of the wave) or a left-hand polarized Alfven wave $\mathbf{\delta B_w} = \delta B\cos(\omega t - k_0x)\mathbf{e_y} - \delta B\sin(\omega t - k_0x)\mathbf{e_z}$ with wave number $k_0c/\omega_{pp} = 0.21$, and the wave propagates along the x direction. $\theta_{k_0B_0}$ denotes the angle between the propagating direction of the pump wave and the ambient magnetic field $\mathbf{B}_0 = B_0(\cos\theta_{k_0B_0}\mathbf{e}_x + \sin\theta_{k_0B_0}\mathbf{e}_y)$ and is called as the propagating angle. The associated bulk velocity is $\mathbf{\delta u}/V_A = -\mathbf{\delta B_w}/B_0$, and the dispersion relation of the pump wave is $\omega = k_0v_A\cos(\theta_{k_0B_0})$. Nine runs are performed. The proton beta β_i, the amplitude of pump wave $\delta B_z/B_0$, the propagating angle $\theta_{k_0B_0}$, and the polarization of pump wave for each run are shown in Table I.

In the simulations, the protons have Maxwellian distributions. The number of grid cells is $n_x \times n_y = 150 \times 150$, and the grid cell size is $\Delta x = \Delta y = 1.0c/\omega_{pp}$. The electron resistive length is set as $L_r = \eta c^2/(4\pi v_A) = 0.02c/\omega_{pp}$. There are average ~1200 macroparticles in every cell for the protons. The time step is $\Omega_p\Delta t = 0.025$.

III. SIMULATION RESULTS

Figure 1 displays the time evolution of (a) the density fluctuations $\langle(\delta\rho/\rho_0)^2\rangle^{1/2}$ (where ρ_0 is the initial density) and (b) the wave energy of the backward Alfven wave E^- (normalized to the initial pump wave energy $E_0 = E^+(t=0)$) and the associated cross-helicity $\sigma_c = (E^+ - E^-)/(E^+ + E^-)$ for run 1. Here, $E^+(E^-)$ refers to the pseudo-energy of the wave propagating forward (backward) according to the Elsässer variables, and the cross-helicity σ_c measures the Alfvenicity of the system.[8,21,26] Density fluctuations begin to increase at $\Omega_pt \approx 1200$, which indicates the excitation of a parametric instability. The instability saturates at $\Omega_pt \approx 2500$ with the amplitude of the density fluctuations $\langle(\delta\rho/\rho_0)^2\rangle^{1/2} \approx 0.03$. With the excitation of the density mode, the energy of backward Alfven waves increases, while the cross-helicity begins to decrease, and it drops to about 0.39 at the end of the simulation. This process is in good agreement with the previous results of a decay instability.[4,8]

Figure 2 shows the characteristics of the $k_x - k_y$ diagram obtained from the fast Fourier transform (FFT) transforming of $\delta\rho/\rho_0$ and $\delta B_z/B_0$ at $\Omega_pt = 0$, 1500, and 2900 for run 1. At $\Omega_pt = 0$, only the parallel propagating pump Alfven wave (bottom left) with the initial wave number $k_0c/\omega_{pp} = 0.21$ exists. With the excitation of the decay instability, a density mode, whose dominant mode is parallel to the ambient magnetic field (also along the propagating direction of the pump wave), is excited, and its wave number is about $k_sc/\omega_{pp} \approx 0.33$, as shown at $\Omega_pt = 1500$. At the same time, a backward daughter Alfven wave (bottom middle), which propagates along the ambient magnetic field, appears. The generation of the daughter Alfven wave is a consequence of a three-wave coupling, and its wave number satisfies the resonant condition $k^- = |k_0 - k_s| \approx 0.12\omega_{pp}/c$. The obliquely propagating density modes and daughter Alfven waves are then excited. After the saturation of the parametric decay, as shown at $\Omega_pt = 2900$ (up right), a broad range of perpendicular wave numbers can be observed. The remarkable property of the wide spectra is that all excited modes have the same k_x. It means that the resonant condition of the three-wave coupling is still satisfied in the parallel direction during the perpendicular decay of the pump wave. The harmonics of the density mode with $k_x \approx 2k_s \approx 0.66\omega_{pp}/c$ can also be found; however, these modes are much weaker and insignificant in the parametric decay.

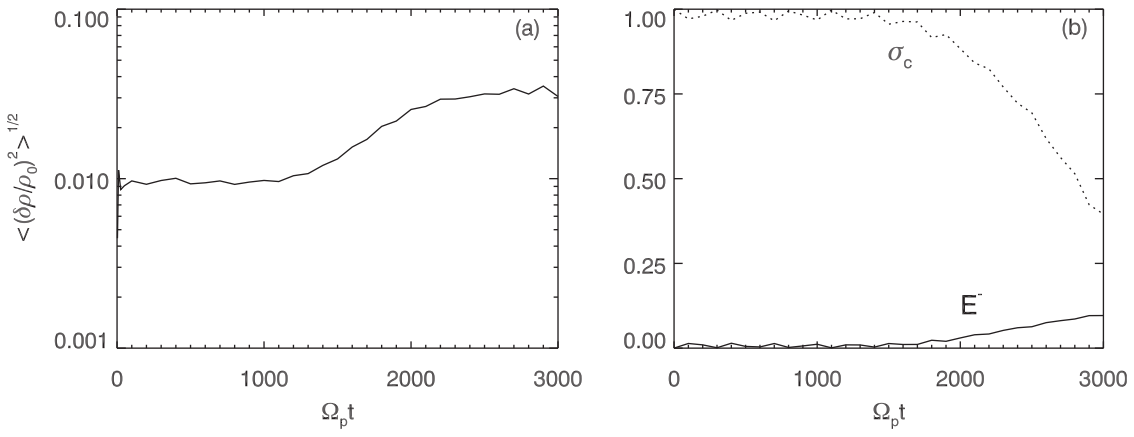

FIG. 1. Time evolution of (a) the density fluctuations $\langle(\delta\rho/\rho_0)^2\rangle^{1/2}$ and (b) the wave energy of backward propagating Alfven waves E^- (solid line), and the associated cross-helicity σ_c (dashed line) for run 1.

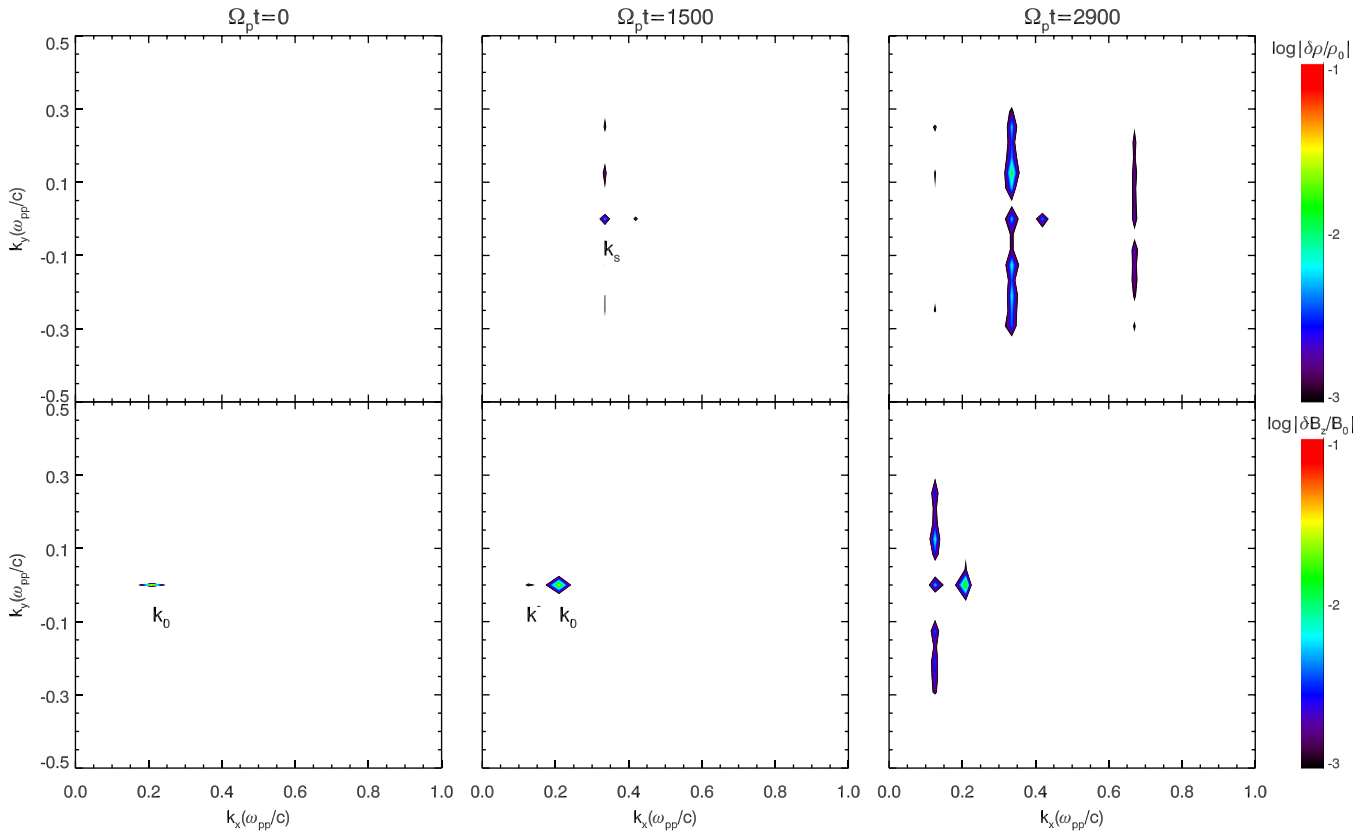

FIG. 2. The contour of characteristics of the $k_x - k_y$ diagram obtained from the FFT transforming of $\delta\rho/\rho_0$ and $\delta B_z/B_0$ at $\Omega_p t = 0$, 1500, and 2900 for run 1. k_0, k_s, and k^- denote the wave number of the pump Alfven wave, the daughter density mode, and the daughter Alfven wave, respectively.

The transverse modulation of the fluctuating density and magnetic field during the parametric decay can be shown more clearly in Fig. 3, which displays the 2-D spatial profile of the fluctuating density $\delta\rho/\rho_0$ and magnetic field component $\delta B_z/B_0$ at $\Omega_p t$ =2900 for run 1. The modulation of the fluctuating density and magnetic field across the ambient magnetic field can be clearly observed, which indicates the production of the obliquely propagating waves.

The effects of the amplitude of the pump wave, the plasma beta, and the propagating angle of the pump wave on the parametric decay are also investigated. Runs 1–3 consider the effects of the amplitude of the pump wave, runs 3–5 investigate the effects of the plasma beta, and runs 6–7 describe the effects of the propagating angle of the pump wave. Figure 4 shows (a) the time evolution of the density fluctuations $\langle(\delta\rho/\rho_0)^2\rangle^{1/2}$, the spectra of (b) the density fluctuations and (c) the daughter Alfven waves versus k_y for runs 1–3. The spectra are calculated as follow: first, a spectrum in the $k_x - k_y$ space is obtained by the FFT and then we obtain the spectra of the density fluctuations and daughter Alfven waves versus k_y at the fixed $k_x c/\omega_{pp} = 0.33$ and 0.12 for the density fluctuations and daughter Alfven waves, respectively. In Figs. 4(b) and 4(c), the spectra are calculated at $\Omega_p t = 2900$, 1800, and 1200 for runs 1, 2, and 3, respectively, and at that time, the perpendicular parametric decay has already saturated. We can find that with the increase of the amplitude of the pump wave, both the linear growth rate and the amplitude of the density fluctuations at the saturation

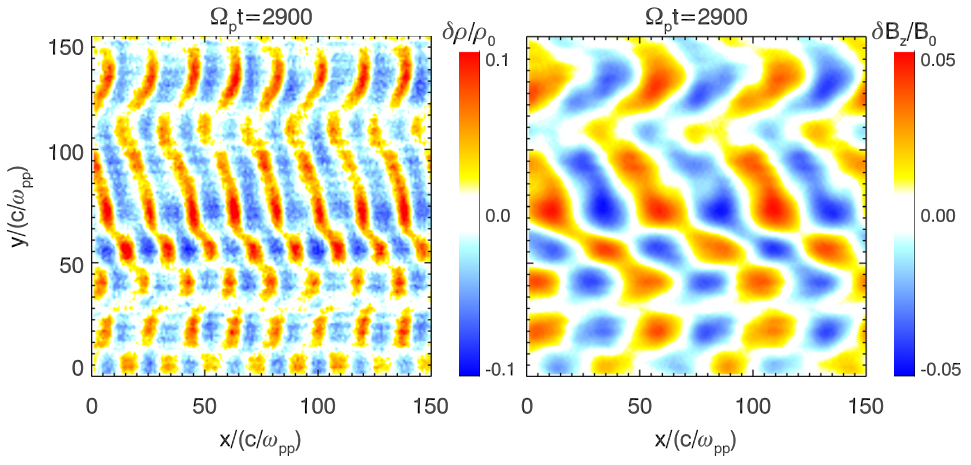

FIG. 3. The 2-D contour plots of the fluctuating density $\delta\rho/\rho_0$ and magnetic field component $\delta B_z/B_0$ at $\Omega_p t$ = 2900 for run 1. Here, the fluctuating magnetic field of pump wave has been removed.

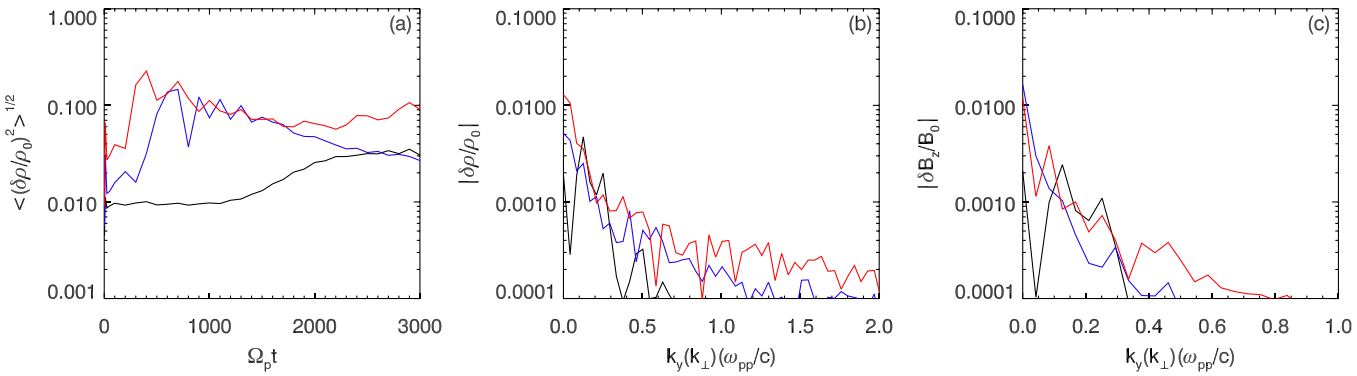

FIG. 4. (a) Time evolution of the density fluctuations $\langle(\delta\rho/\rho_0)^2\rangle^{1/2}$, the spectra of (b) the density fluctuations and (c) the magnetic field fluctuations versus k_y ($k_\perp$) at $\Omega_p t = 2900$, 1800, and 1200 for runs 1 (black lines), 2 (blue lines), and 3 (red lines).

stage of the instability increase, and the range of their wave numbers in the perpendicular direction becomes broad.

In Fig. 5, we illustrate (a) the time evolution of the density fluctuations $\langle(\delta\rho/\rho_0)^2\rangle^{1/2}$, the spectra of (b) the density fluctuations and (c) the daughter Alfven waves versus k_y at $\Omega_p t = 1200$, 1300, and 2200 for runs 3, 4 and 5, respectively. The time is chosen when the parametric decay has saturated. The spectra are calculated as in Fig. 4. With the increase of the plasma beta, the linear growth rate of the parametric decay decreases; however, its effects on the amplitude of the density fluctuations at the saturation stage are almost negligible. At the same time, the range of the spectra for both the density fluctuations and daughter Alfven waves in the perpendicular direction almost does not change.

The decay of an oblique pump wave is also studied in this paper. Figure 6 displays the characteristics of the $k_x - k_y$ diagram obtained from the FFT transforming of $\delta\rho/\rho_0$ and $\delta B_z/B_0$ at $\Omega_p t = 0$, 700, and 1200 for run 7. We can find that with the excitation of the parametric decay, both the density mode k_s (up middle) and daughter Alfven mode k^- (bottom middle) can be observed. Consistent with the results of Matteini *et al.*,[26] the parametric decay initially takes place along the propagating direction of the pump wave, and it satisfies the three-wave coupling condition $k^- = |k_0 - k_s| \approx |0.21 - 0.33| = 0.12\omega_{pp}/c$. After the saturation of the decay, a broad spectral range of both the magnetic (bottom right) and density (up right) fluctuations in the perpendicular direction can be observed.

Figure 7 shows (a) the time evolution of the density fluctuations $\langle(\delta\rho/\rho_0)^2\rangle^{1/2}$, the spectra of (b) the density fluctuations and (c) the daughter Alfven waves versus $k_\perp$ at $\Omega_p t = 1800$, 1500, and 1100 for runs 2, 6, and 7, respectively. A spectrum in the $k_x - k_y$ space is first obtained by the FFT, and then it is converted to the $k_\parallel - k_\perp$ space. At last, the spectrum of the density fluctuations and daughter Alfven waves versus $k_\perp$ is obtained at the fixed $k_\parallel c/\omega_{pp} = 0.33\cos(\theta_{k_0B_0})$ and $0.12\cos(\theta_{k_0B_0})$ for the density fluctuations and daughter Alfven waves, respectively. We can find that with the increase of the propagating angle of the pump wave, the spectral range of the excited waves in the perpendicular direction becomes broad. However, its effects on both the linear growth rate and the amplitude of the decay are negligible.

Next, we investigate the parametric decay of a left-hand polarized pump Alfven wave. Figure 8 displays the time evolution of (a) the density fluctuations $\langle(\delta\rho/\rho_0)^2\rangle^{1/2}$ (where ρ_0 is the initial density) and (b) the wave energy of the backward Alfven wave E^-(normalized to the initial pump wave energy $E_0 = E^+(t=0)$) and the associated cross-helicity $\sigma_c = (E^+ - E^-)/(E^+ + E^-)$ for run 8. Density fluctuations begin to increase at $\Omega_p t \approx 150$ and saturate at $\Omega_p t \approx 500$ with the amplitude of the density fluctuations $\langle(\delta\rho/\rho_0)^2\rangle^{1/2} \approx 0.25$. With the excitation of the density mode, the energy of the backward Alfven waves also increases. Both the density fluctuations and the excitation of the backward waves indicate the occurrence of the decay instability, which results in a drop of the cross-helicity to -0.9.

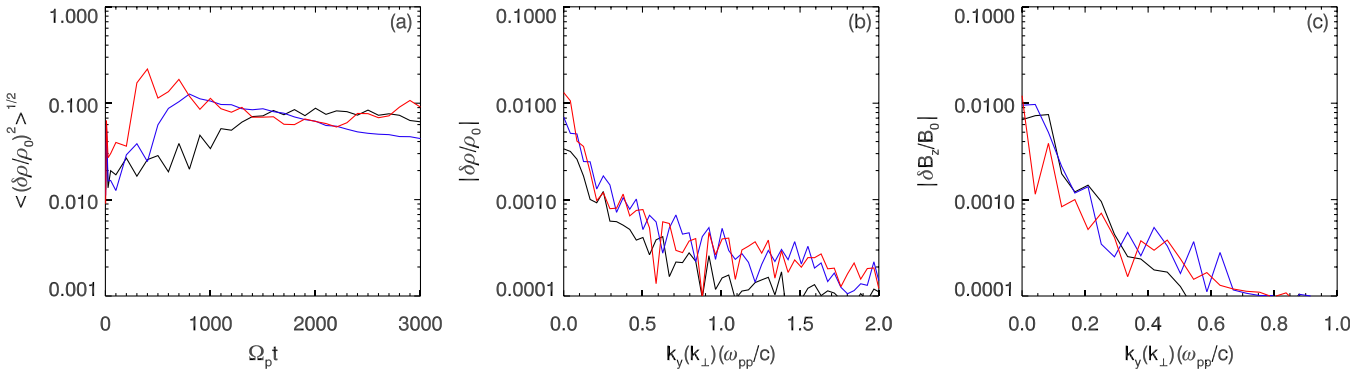

FIG. 5. (a) Time evolution of the density fluctuations $\langle(\delta\rho/\rho_0)^2\rangle^{1/2}$, the spectra of (b) the density fluctuations and (c) the magnetic field fluctuations versus k_y ($k_\perp$) at $\Omega_p t$ =1200, 1300, and 2200 for runs 3 (red lines), 4 (blue lines) and 5 (black lines).

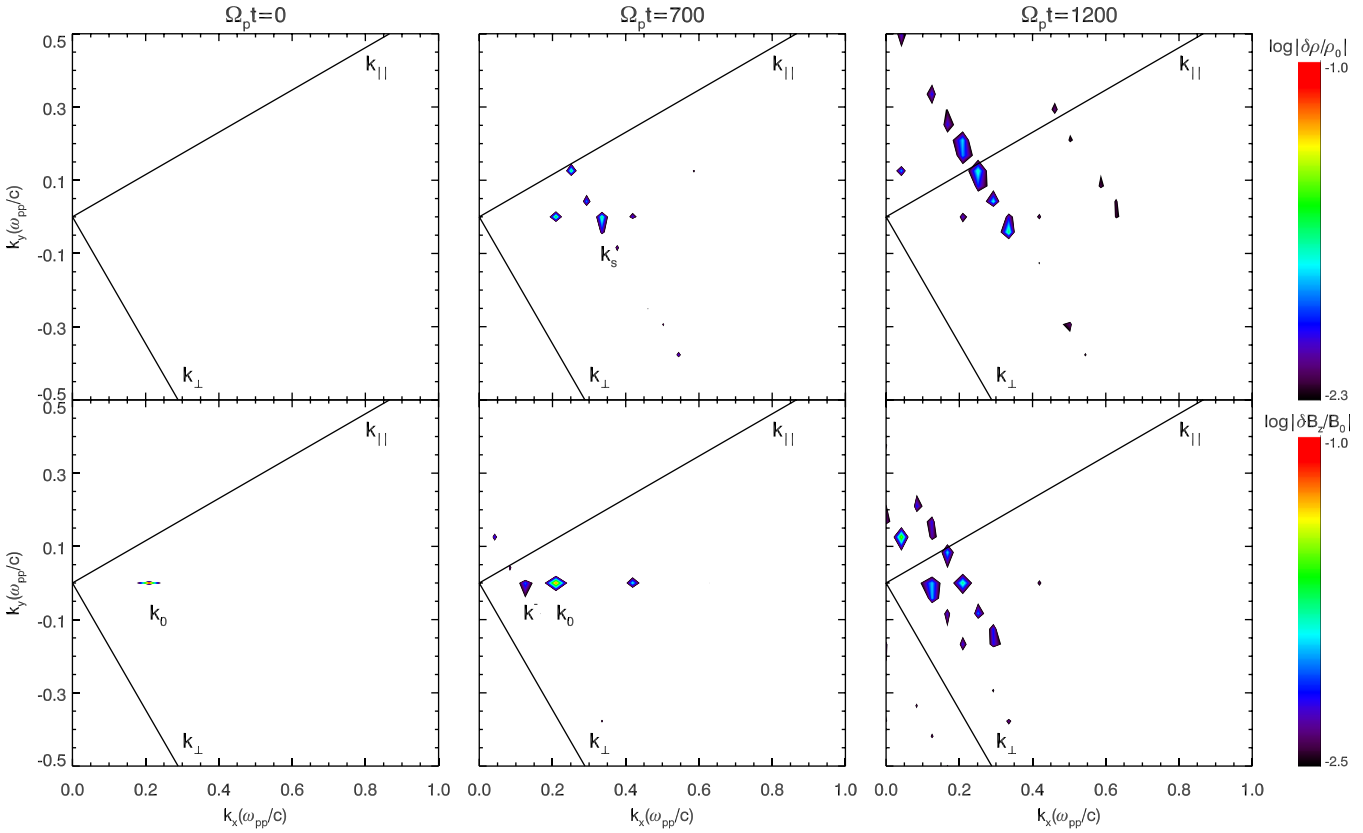

FIG. 6. The contour of characteristics of the $k_x - k_y$ diagram obtained from the FFT transforming of $\delta\rho/\rho_0$ and $\delta B_z/B_0$ at $\Omega_p t = 0$, 700, and 1200 for run 7. k_0, k_s, and k^- denote the wave number of the pump Alfven wave, the daughter density mode, and the daughter Alfven wave, respectively. The black lines represent the $k_\parallel - k_\perp$ frame.

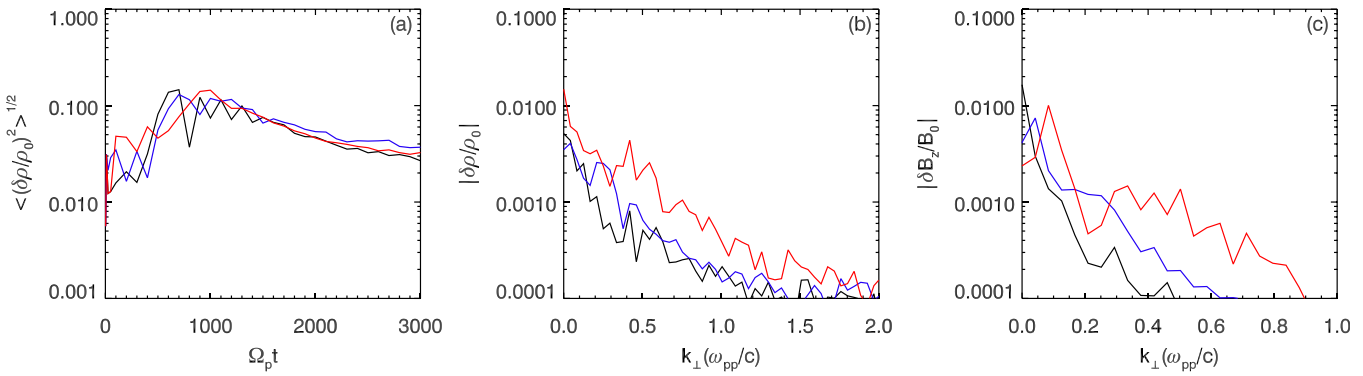

FIG. 7. (a) Time evolution of the density fluctuations $\langle(\delta\rho/\rho_0)^2\rangle^{1/2}$, the spectra of (b) the density fluctuations and (c) the magnetic field fluctuations versus $k_\perp$ at $\Omega_p t$ =1800, 1500, and 1100 for runs 2 (red lines), 6 (blue lines), and 7 (black lines).

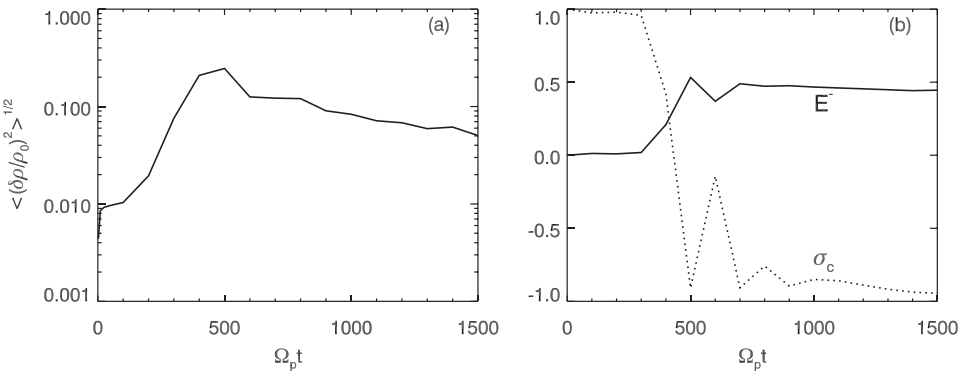

FIG. 8. Time evolution of (a) the density fluctuations $\langle(\delta\rho/\rho_0)^2\rangle^{1/2}$ and (b) the wave energy of backward propagating Alfven waves E^- (solid line), and the associated cross-helicity σ_c (dashed line) for run 8.

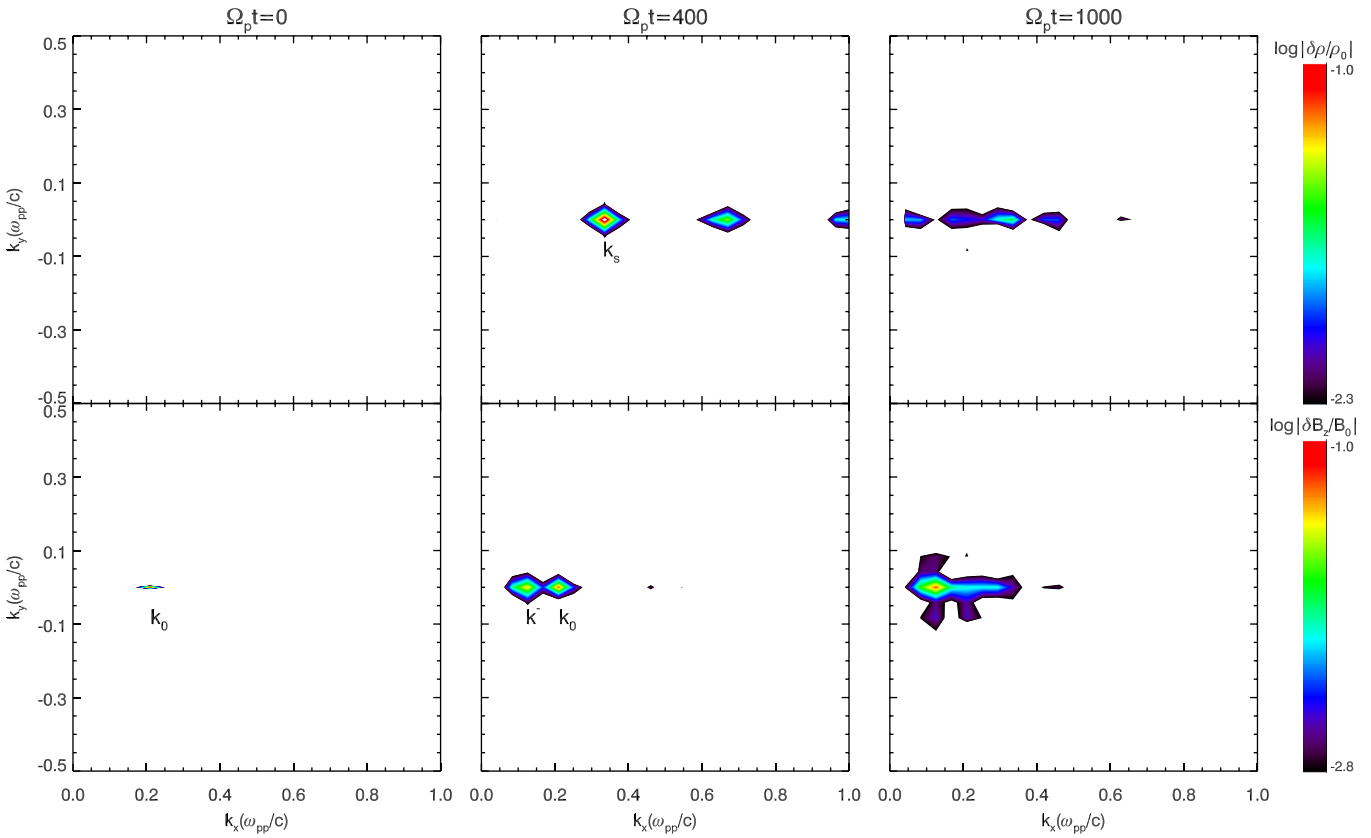

FIG. 9. The contour of characteristics of the $k_x - k_y$ diagram obtained from the FFT transforming of $\delta\rho/\rho_0$ and $\delta B_z/B_0$ at $\Omega_p t = 0$, 400, and 1000 for run 8. k_0, k_s, and k^- denote the wave number of the pump Alfven wave, the daughter density mode, and the daughter Alfven wave, respectively.

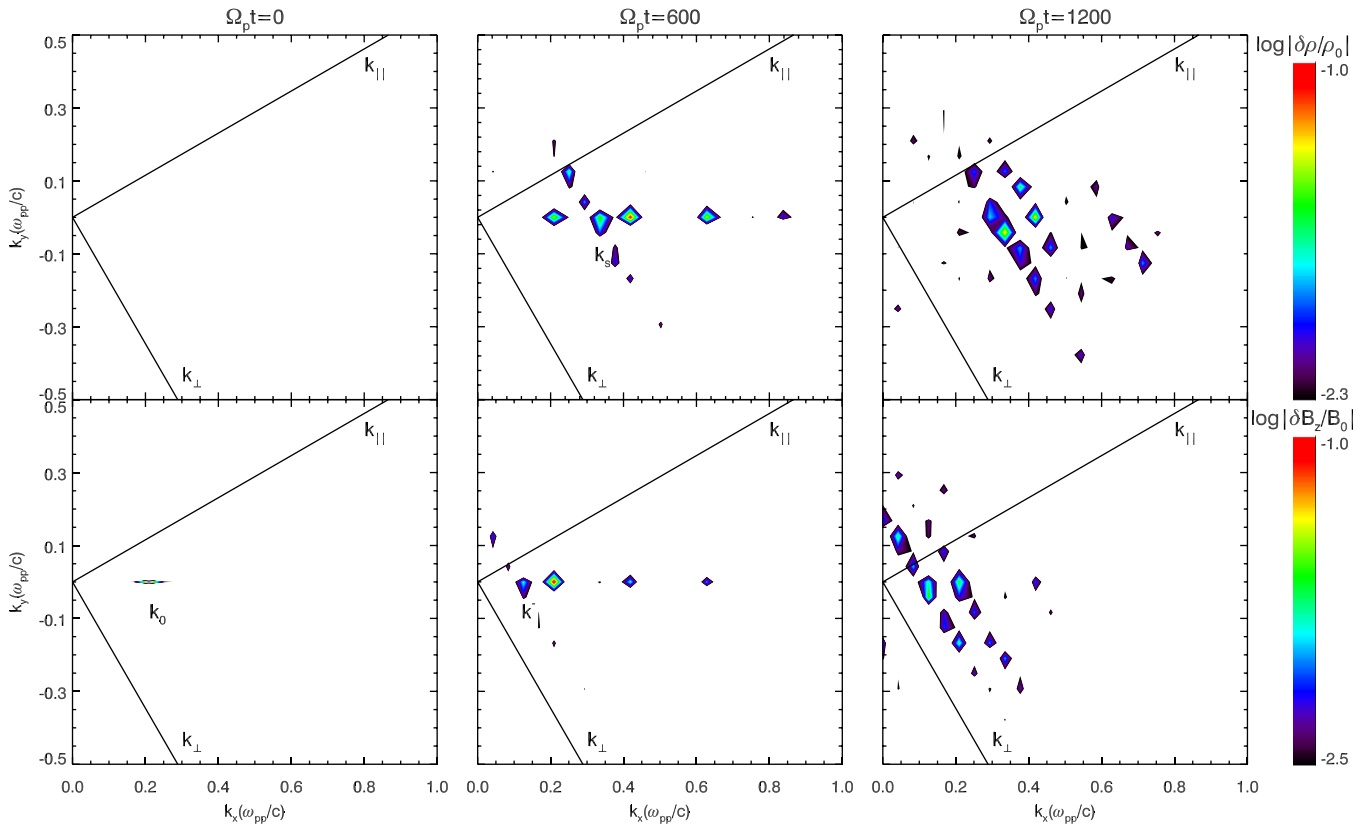

FIG. 10. The contour of characteristics of the $k_x - k_y$ diagram obtained from the FFT transforming of $\delta\rho/\rho_0$ and $\delta B_z/B_0$ at $\Omega_p t = 0$, 600, and 1200 for run 9. k_0, k_s, and k^- denote the wave number of the pump Alfven wave, the daughter density mode, and the daughter Alfven wave, respectively. The black lines represent the $k_\parallel - k_\perp$ frame.

Figure 9 illustrates the characteristics of the $k_x - k_y$ diagram obtained from the FFT transforming of $\delta\rho/\rho_0$ and $\delta B_z/B_0$ at $\Omega_p t = 0$, 400, and 1000 for run 8. At $\Omega_p t = 0$, only the parallel propagating pump Alfven wave (bottom left) with the initial wave number $k_0 c/\omega_{pp} = 0.21$ exists. With the excitation of the decay instability, both a density mode $k_s c/\omega_{pp} \approx 0.33$ and a backward daughter Alfven $k^- c/\omega_{pp} \approx 0.12$ appear along the ambient magnetic field (also along the propagating direction of the pump wave k_0), as shown at $\Omega_p t = 400$. The parametric decay is the process of three-wave coupling, and the above wave numbers satisfy the resonant condition: $k^- = |k_0 - k_s|$. Unlike the decay instability of the linearly polarized Alfven wave in Fig. 2, no strong perpendicular decay is observed in this simulation. As shown at $\Omega_p t = 1000$, both the dominant density and magnetic modes propagate mainly along the ambient magnetic field.

We also show the parametric decay of the obliquely propagating pump wave with left-hand polarization in Fig. 10, which displays the characteristics of the $k_x - k_y$ diagram obtained by the FFT transforming of $\delta\rho/\rho_0$ and $\delta B_z/B_0$ at $\Omega_p t$=0, 600, and 1200 for run 9. We can find that the parametric decay initially takes place along the propagating direction of the pump wave, and both the density mode k_s (up middle) and daughter Alfven mode k^- (bottom middle) are excited, which propagate mainly along the initial propagating direction and satisfy the three-wave coupling condition $k^- = |k_0 - k_s| \approx |0.21 - 0.33| = 0.12\omega_{pp}/c$. After the saturation of the decay, the strong perpendicular decay can also be observed, and there is a broad spectral range of both the magnetic (bottom right) and density (up right) fluctuations in the perpendicular direction.

IV. CONCLUSION AND DISCUSSIONS

By employing 2-D hybrid simulations, the parametric decay of a monochromatic Alfven waves in low beta plasma is investigated. The decay first occurs along the propagating direction of the pump wave, and both a forward density mode and a backward daughter Alfven wave are excited, which satisfy the resonant condition of a three-wave coupling. For a linearly polarized pump wave, either a parallel or obliquely propagating wave can lead to the decay along the perpendicular direction, while for a left-hand polarized pump wave, only an obliquely propagating wave can generate the perpendicular decay. Recently, Verscharen *et al.*[30] have also investigated the parametric decay of oblique Alfven waves in two-dimension hybrid simulations. In their simulation, the daughter waves are found to be mainly along the initial propagating direction of the pump wave and they conjecture that the initial wave propagating vector is the most important guiding direction and will determine the daughter wave propagation vector. However, our results show that besides the decay along the initial propagating direction, the perpendicular decay is also noteworthy. Their different results are probably due to the short time period ($\sim 500\,\Omega_p^{-1}$) in their simulations.

The obliquely propagating Alfven waves are considered to be able to stochastically heat the plasma and may have relevance for the heating of ions in the solar corona.[31–34] Our simulations imply that the parametric decay of a parallel or obliquely pump Alfven wave provides a mechanism for the generation of obliquely propagating Alfven waves, and its role in the plasma heating is our future investigation.

ACKNOWLEDGMENTS

This research was supported by the National Science Foundation of China, Grant Nos. 41174124, 41274144, 40931053, 41121003, the 973 Program (2012CB825602), CAS Key Research Program KZZD-EW-01, and Ministry of Education (Grant No. IRT1190).

[1]M. Velli and F. Pruneti, Plasma Phys. Controlled Fusion **39**, B317 (1997).
[2]R. Bruno and V. Carbone, Living Rev. Solar Phys. **2**, 4 (2005).
[3]M. L. Goldstein, J. P. Eastwood, R. A. Treumann, E. A. Lucek, J. Pickett, and P. Decreau, Space Sci. Rev. **118**, 7 (2005).
[4]B. Bavassano, E. Pietropaolo, and R. Bruno, J. Geophys. Res. **105**, 15959, doi:10.1029/1999JA000276 (2000).
[5]J. W. Belcher and L. Davis, Jr., J. Geophys. Res. **76**, 3534, doi:10.1029/JA076i016p03534 (1971).
[6]H. Umeki and T. Terasawa, J. Geophys. Res. **97**, 3113, doi:10.1029/91JA02967 (1992).
[7]C.-Y. Tu and E. Marsch, Space Sci. Rev. **73**, 1 (1995).
[8]F. Malara, L. Primavera, and P. Veltri, Nonlinear Processes Geophys. **8**, 159 (2001).
[9]A. A. Galeev and V. N. Oraevskii, Sov. Phys. Dokl. **7**, 998 (1963).
[10]R. Z. Sagdeev and A. A. Galeev, *Nonlinear Plasma Theory* (Benjamin, New York, 1969).
[11]M. L. Goldstein, Astrophys. J. **219**, 700 (1978).
[12]T. Terasawa, M. Hoshino, J. Sakai, and T. Hada, J. Geophys. Res. **91**, 4171, doi:10.1029/JA091iA04p04171 (1986).
[13]M. Hoshino and M. L. Goldstein, Phys. Fluids B **1**, 1405 (1989).
[14]Y. Nariyuki, S. Matsukiyo, and T. Hada, New J. Phys. **10**, 083004 (2008).
[15]V. Jayanti and J. V. Hollweg, J. Geophys. Res. **98**, 19049, doi:10.1029/93JA02208 (1993).
[16]L. Gomberoff, K. Gomberoff, and A. L. Brinca, J. Geophys. Res. **106**, 18713, doi:10.1029/2000JA000384 (2001).
[17]Y. Nariyuki, T. Hada, and K. Tsubouchi, Phys. Plasmas **14**, 122110 (2007).
[18]Y. Nariyuki, T. Hada, and K. Tsubouchi, J. Geophys. Res. **114**, A07102, doi:10.1029/2009JA014178 (2009).
[19]J. A. Araneda, E. Marsch, and A. F. Vinas, Phys. Rev. Lett. **100**, 125003 (2008).
[20]J. A. Araneda, Y. Maneva, and E. Marsch, Phys. Rev. Lett. **102**, 175001 (2009).
[21]L. Matteini, S. Landi, M. Velli, and P. Hellinger, J. Geophys. Res. **115**, A09106, doi:10.1029/2009JA014987 (2010).
[22]A. F. Vinas and M. L. Goldstein, J. Plasma Phys. **46**, 129 (1991).
[23]S. Ghosh, A. F. Vinas, and M. L. Goldstein, J. Geophys. Res. **98**, 15561, doi:10.1029/93JA01534 (1993).
[24]S. Ghosh and M. L. Goldstein, J. Geophys. Res. **99**, 13315, doi:10.1029/94JA00474 (1994).
[25]L. Del Zanna, M. Velli, and P. Londrillo, Astron. Astrophys. **367**, 705 (2001).
[26]L. Matteini, S. Landi, L. Del Zanna, M. Velli, and P. Hellinger, Geophys. Res. Lett. **37**, L20101, doi:10.1029/2010GL044806 (2010).
[27]D. Winske, Space Sci. Rev. **42**, 53 (1985).
[28]K. B. Quest, J. Geophys. Res. **93**, 9649, doi:10.1029/JA093iA09p09649 (1988).
[29]D. Winske and N. Omidi, *Computer Space Plasma Physics: Simulation Techniques and Software* (Terra Sci. Publishers, Tokyo, 1993).
[30]D. Verscharen, E. Marsch, U. Motschmann, and J. Muller, Phys. Rev. E **86**, 027401 (2012).
[31]X. L. Gao, Q. M. Lu, X. Li, C. Huang, and S. Wang, Phys. Plasmas **19**, 032901 (2012).
[32]X. L. Gao, Q. M. Lu, X. Li, L. C. Shan, and S. Wang, Astrophys. J. **764**, 71 (2013).
[33]X. Li and Q. M. Lu, J. Geophys. Res. **115**, A08105, doi:10.1029/2010JA015303 (2010).
[34]Q. M. Lu and L. Chen, Astrophys. J. **704**, 743 (2009).